Strength and Behaviour of Spruce-Pine Glulam Timber Moment Connections Using Glued-in Steel Rods.

Étienne Gauthier-Turcotte[1], Sylvain Ménard[2] and Mathieu Fiset[3]

Abstract:

This paper presents experimental testing on glulam beam-column moment resisting connections using glued-in rods and compares results with model predictions. Three connections geometries, in term of number of rods and member size, were tested and compared.

Experimental results showed the high efficiency of glued-in rods connections to transfer loads and bending moment between spruce-pine glulam timber members. It was found that the tested connections behave as a semi-rigid moment-resisting connection and may experience a ductile failure mode when properly designed. The observed failure modes of the connections were related to steel rods failure or wood splitting of the anchorage.

Comparison of experimental results with model predictions showed good agreement.

Keywords: Glued-in Rods; Moment resisting connection; Glulam timber; Beam-column connections; Stress distribution.

Introduction

Wood is increasingly used in construction due to its good environmental and architectural properties (Brassard 2018, Cecobois 2018). To build larger and more resistant structures, it is necessary to develop connections able to withstand the forces induced on the beams and columns.

[1] Étienne Gauthier, Université du Québec à Chicoutimi, Québec, Canada, etienne.gauthier-turcotte1@uqac.ca
[2] Sylvain Ménard, Ph.D., Université du Québec à Chicoutimi, Québec, Canada, sylvain_menard@uqac.ca
[3] Mathieu Fiset, Ph.D., Université du Québec à Chicoutimi, Québec, Canada, mathieu_fiset@uqac.ca

Glued-in rods (GiRod) connections offer several advantages in terms of mechanical properties, fire resisting capacity and architectural design. This type of connection consists in rods inserted in pre-drilled holes in the timber members and bonded to the wood with an adhesive (see Fig. 1).

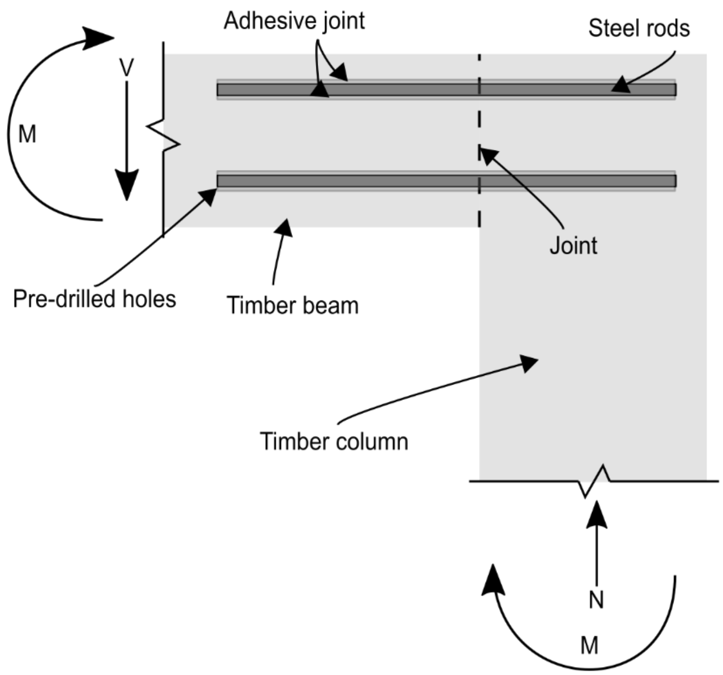

Fig. 1. Typical glued-in rods connection

Glued-in rod connections have been used since the 1970s (Klapwijk 1978, Tlustochowicz, Serrano et al. 2010, Verdet 2017) but remain relatively unknown and the lack standard specifications limits their using. However, the mechanical performance and the architectural properties exhibited by that type of connection are increasingly sought after and much research has been carried out in recent years. Several researchers have investigated the pull-out strength of rods used in moment connections installed parallel and perpendicular to the grain (Widmann, Steiger et al. 2007, Inoue, Uetsuki et al. 2018, Kajikawa, Hiraga et al. 2018) and various models were proposed (Stepinac 2013, Stepinac, Bidakov et al. 2018). Others investigated long-term behaviour and the effect of temperature variations on glued-in rods connections and mainly showed strength and failure behaviours variations related to the adhesive capacity (Lartigau 2013).

Current limitations for design

The main limitation surrounding the use of glued-in rod connections stems from the lack of experimental results. To the authors knowledge, very few researchers studied moment-resisting glued-in rods connections concerning the maximum moments that can be taken up by different configurations as well as their rotational stiffness.

A second limitation is related to the lack of standard design specifications. Several studies report a non-uniform tensile and bond stresses along the anchored rods and stress peaks at their both ends (Hassanieh, Valipour et al. 2018). This stresses distribution makes connection behaviour and strength difficult to predict. An improved comprehension of the stresses distribution along the anchored rods would help to better understand the connection behaviour and provide future design guidance.

Aims

To the authors' knowledge, there is very little documentation regarding moment resisting beam-column connection using glued-in rods (Oh 2016). The main objective of this paper is to study the mechanical behaviour of glued-in rods connections subjected to bending moment and provide reliable experimental results that will serve as a solid basis to support future design guidelines.

To do so, this research aimed to study the connection ability to carry bending moment and shear, and the resulting axial and bond stresses distribution in multi-rod connections with true scale experimental testing.

Theoretical background

Glued-in steel rods installed in Spruce-pine glulam timber was previously studied by several researches (Vasek 2008, Ouellet 2013, Bédard-Blanchet 2014). Most studied the behaviour of a glued-in steel rod installed parallel to the grain with pull-out tests. They found that the stress distribution along the anchor is non-linear and may influence their failure mode and capacity. They determined the different possible failure modes and proposed theoretical models predicting the maximum pull-out capacity according to various parameters, such as the materials properties and the components geometry.

Other researchers studied the behaviour of glued-in steel rods group installed in timber with pull-out test. They proposed rods spacing limitations and minimum cover to avoid brittle wood splitting failure. The limitations proposed by experts and standards (Simonin 2008, DIN 2012) are presented in Fig.2. In this figure, d_r is the rod diameter, e_d is the minimum edge distance and S is the spacing between two consecutive rods axis.

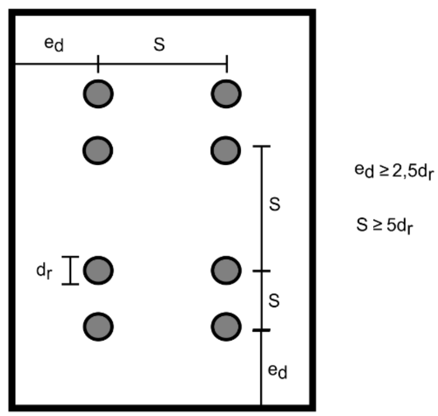

Fig. 2. Rods spacing limitations proposed by (DIN 2012), (Simonin 2008) and others.

Pull-out strength

Several models have been proposed (Stepinac 2013) to determine pull-out capacity, R_a, of glued-in steel rods. Generally, these models can be expressed as follows:

$$R_a = \pi \cdot d_h \cdot l_a \cdot f_{b,a} \leq A_r \cdot f_u \tag{1}$$

With d_h the hole diameter, l_a the embedded length of the anchorage, $f_{b,a}$ the bond strength, A_r the rod net area and f_u the rod tensile strength. Most of the tests to determine the bond strength were carried out on rods installed parallel to the grain and showed the timber generally limits the bond strength.

However, in beam-column structural connections subjected to bending moment, it is rather relevant to consider the pull-out strength of rod installed perpendicularly to the grain.

Researchers (Gauthier-Turcotte, Menard et al. 2021) previously conducted experimental pull-out tests on single glued-in steel rod installed perpendicularly to the grain of spruce-pine glulam timber. Tests parameters and main results are presented in Table 1 (average of 7 tests).

Table 1. Pull-out tests parameters and average strength of rods installed perpendicularly to the grain in spruce-pine glulam timber determined by (Gauthier-Turcotte, Menard et al. 2021).

l_a (mm)	d_r (mm)	A_r (mm^2)	d_h (mm)	Steel grade	R_a (kN)	Failure type
300	15.9	145.8	19.1	ASTM A307 A	66.4	Ductile steel failure
				ASTM A193 B7	81.8	Brittle wood failure

Theoretical models for the calculation of column-beam connections

In terms of moment transfer in beam-column connections, previous studies (Fragiacomo and Batchelar 2012) proposed a model to determine each connection component stresses to determine the connection moment capacity as presented in Fig. 3. By using this model, the force taken up by the steel rods in tension, the steel rods in compression and the wood in compression are calculated. The moment carry by the connection is then determined from the forces carry by each component.

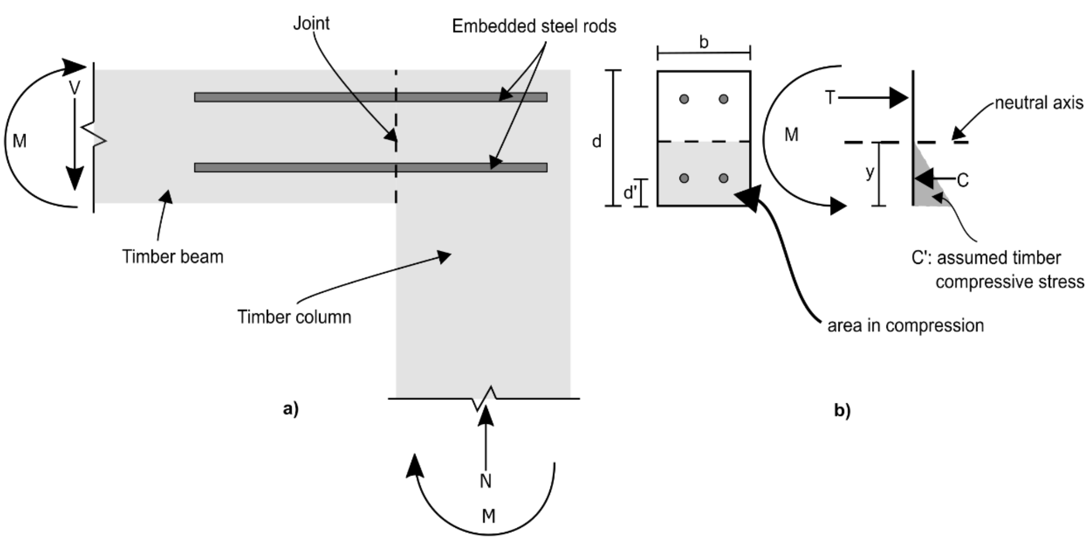

Fig. 3. a) glued-in rods connection and b) mechanical behaviour of the section located at the junction between the beam and the column and associated stress components

In Fig. 3, *T* and *C* are the forces carried by the steel rods in tension and in compression, respectively, *C'* is the resulting force carried by the wood in compression and *y* indicates the depth of the neutral axis determined from equilibrium. At the face of the column, M is the bending moment transferred by the connection, which is in equilibrium with the load supported by the structure. By considering elastic behaviour of materials, the axial stress, σ, carried by each component may be determine as follows,

$$\sigma = n \cdot \frac{M \cdot y}{I} \tag{2}$$

Where *n* is Young modulus ratio between materials (*n* = 1 for σ determined for the wood and n = E_s/E_w for σ determined for the steel rods, with E_s and E_w the steel and wood Young modulus, respectively), *I* the inertia of the section and *y* the distance between the neutral axis and the considered component.

Once the stresses are determined for each component, the forces may be determined as follows:

$$T = A_s \cdot \sigma_s \tag{3}$$

$$C' = A'_s \cdot \sigma'_s \tag{4}$$

$$C' = \frac{1}{2} \cdot \sigma_w \cdot b \cdot y \tag{5}$$

Where σ_s, σ'_s and σ_w refer to the axial stresses determined form Eq. (2) for the steel rods in compression, the steel rods in tension and the wood in compression, respectively, and A_s and A'_s are the total steel rods area in tension and in compression, respectively.

Experimental program

Specimens

In order to study the behaviour of glued-in steel rods moment-connections, three series of true-scale experimental tests were carried out. For each series, 7 samples of spruce-pine glulam timber structural element were built and tested until failure. The chosen structural element represented a beam and a column connected with glued-in steel rods. In this study, the main parameters were the number of rods and the dimensions of the beam section selected to respect minimum spacings (see Fig. 2). The geometry of each series is presented in Fig. 4 and Table 2.

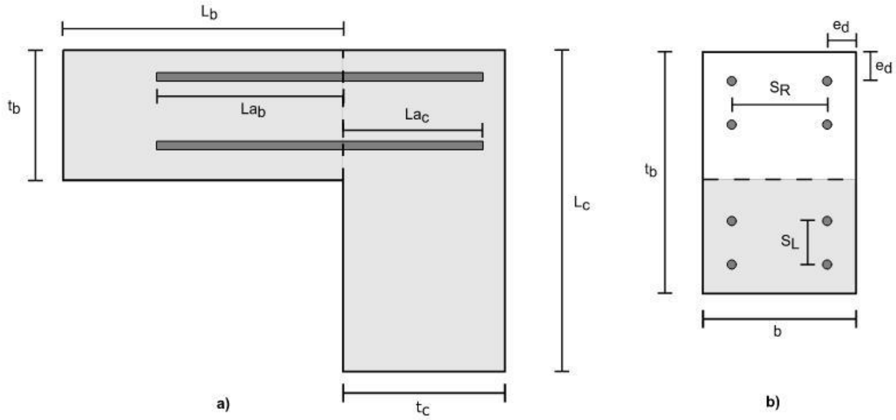

Fig. 4. Specimen geometrical parameters

In Fig. 4, the subscripts *b* and *c* to the beam and the column, respectively. L_b and L_c are the length of the beam and the column, La_b and La_c the anchorage length in the beam and the column, t_b and t_c the thickness of the beam and the column, *b* the width of the connection, S_R the spacing of the rods on a same row, S_L the spacing of the rows and e_d the edge distances.

Table 2. Specimen geometrical parameters (values in mm)

Series	Number of rods	L_b	L_c	La_b	La_c	t_b	t_c	b	S_R	S_L	e_d
1	2					243		130	-	-	
2	4	2000	1000	400	300	243	347	174	74	-	50
3	8					416		265	165	75	

Materials

Spruce-pine glulam graded 20f-EX were used for beams and columns. The timber mechanical characteristic properties of this material, according to CSA 086 (CSA 2019) are: bending strength, f_b, of 25.6 MPa, shear strength, f_v, of 1.75 MPa, compressive strength, f_c, of 25.2 MPa, compressive strength perpendicular to the grain, f_{cp}, of 5.8 MPa, tensile strength perpendicular to the grain, f_{tp}, of 0.51 MPa and Young modulus, E_w, of 10 300 MPa.

According to ASTM D2555 (ASTM 2017a), the average shear strength of the timber, $f_{v.avg}$, may be taken as 5.5 MPa.

For the connection between the beam and the column, ASTM A307 (ASTM 2021) threaded steel rods (specified tensile strength of 414 MPa) with a diameter, d_r, of 15.9 mm were used. To determine average steel yielding and tensile strength, 98 rods were tested according to ASTM E8-E8M (ASTM 2016a) for each steel batch. For the steel used for test series 1 and 2, the average yielding strength, f_y, is 410 MPa (standard deviation, std, of 9 MPa) and the average tensile strength, f_u, is 473 MPa (std = 9 MPa). For the test series #3, f_y = 600 MPa (std = 18 MPa) and f_u = 675 MPa (std = 30 MPa). For all rods, the steel Young modulus, E_s, is taken as 200 000 MPa.

To bond the steel rods to the wood elements, a two-component polyurethane adhesive was used. The mechanical properties of the adhesive used in steel-wood connections given by the manufacturer (Loctite 2015) are presented in Table 3.

Table 3. Mechanical properties of the adhesive (in MPa)

$f_{t.a}$	$f_{c.a}$	$f_{v.a}$	E_a
25 – 30	79.9	2.4 – 3.8	1 560

In this table, $f_{t.a}$, $f_{c.a}$, $f_{v.a}$ and E_a refer to the tensile strength, the compressive strength, the shear strength and the Young modulus of the adhesive, respectively.

Test Method

Fig. 5 presents the experimental testing setup of a beam-column moment connection.

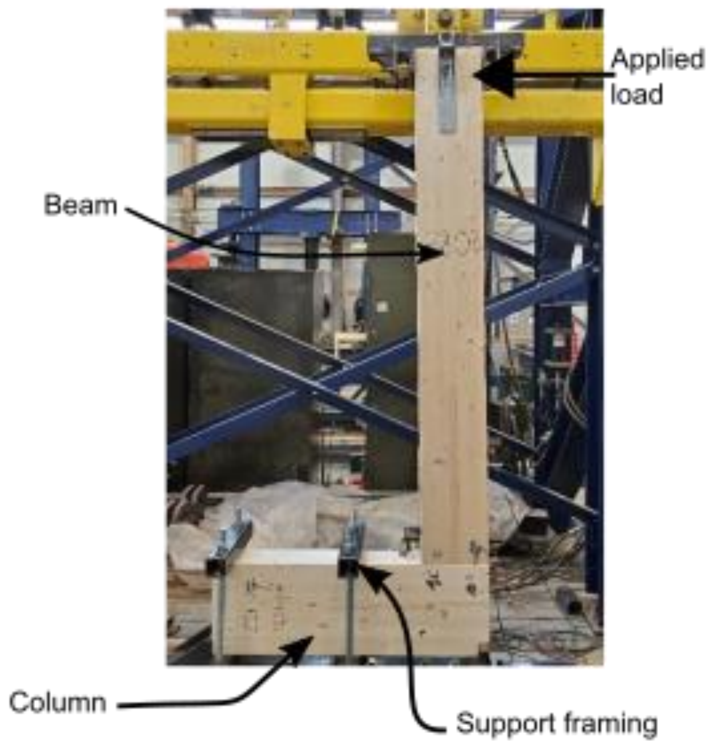

Fig. 5. Experimental set-up

It can be observed that the column was installed horizontally while the beam element was installed vertically. The load was applied at the top of the beam, at a distance L_b between the joint and the load location (refer to Table 2), and in accordance with ASTM E2126 (ASTM 2019) at a rate of 12.7 mm/min (displacement controlled) until failure. The column was retained by a steel framing set-up so that the applied load creates a negative moment and a shear force at the face of the column, which represents typical structural beam-column moment connection (see Fig. 3). A similar loading procedure was initially followed (Verslype 2016) to test glued-in rod column base connections and provided representative results.

In order to determine the rotation of the joint as well as the slip between the column and the beam, three lasers were installed at different locations (see Fig. 6).

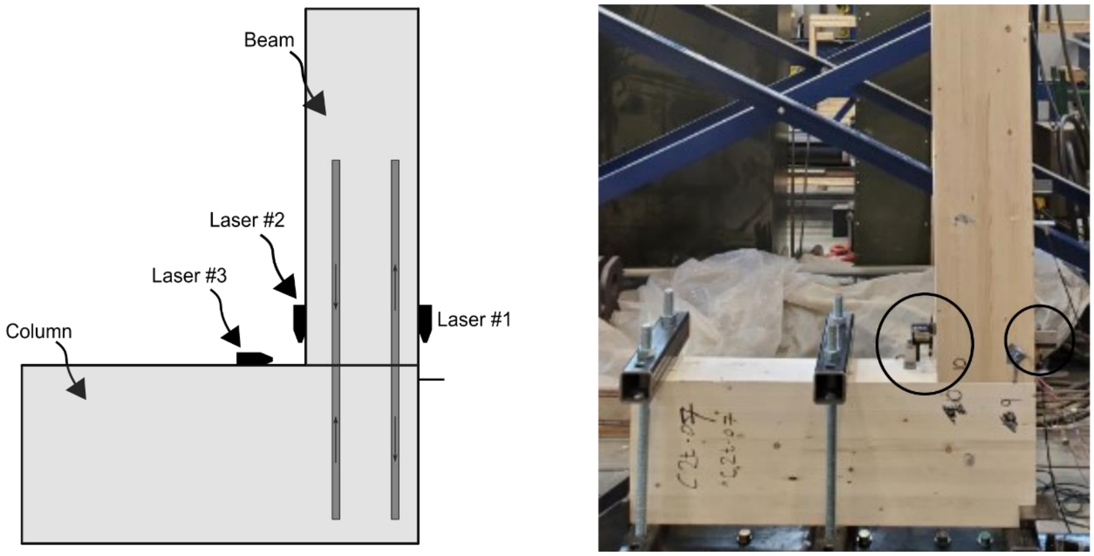

Fig. 6. Laser's positioning

Lasers #1 and #2 were used to determine the rotation between the beam and the column while Laser #3 was used to measure the relative slip of the joint.

Strain gauges were installed at specific locations along the steel rods (see Fig. 7) to measure axial bar strain during tests. As presented in Fig. 7a for the test series #1, 5 strain gauges were installed along the rod in tension, including one at the joint latter used to determine the force carried by the rod at the joint. For the same purpose, a strain gauge was positioned directly at the joint between the beam and the column for all rods in series #2 and selected rods in series #3 (see Fig. 7b and c).

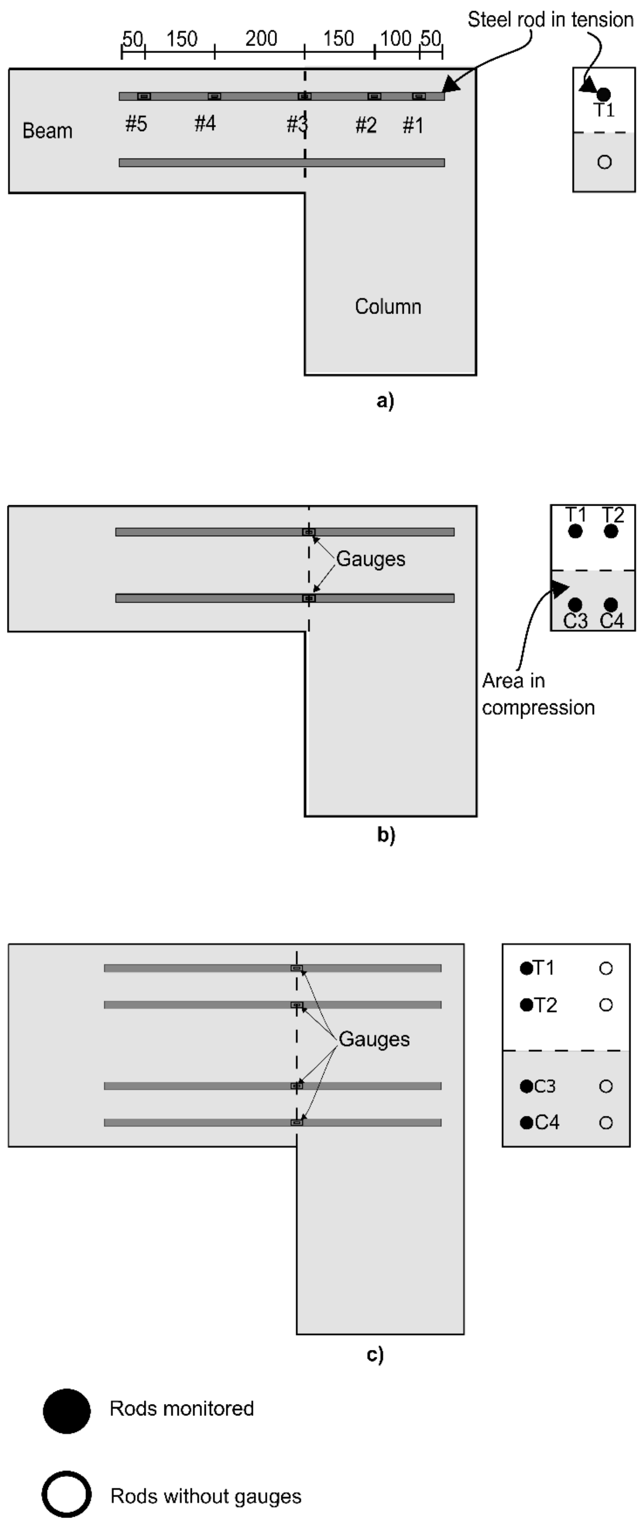

Fig. 7. Location of the strain gauges for a) test series #1, b) series #2 and c) series #3

Results

Members response

Fig. 8 shows the moment versus beam-displacement response of the test series #1 with 2 rods, #2 with 4 rods and #3 with 8 rods. The moment corresponds to the applied load multiplied by the beam length (refer to Table 2) while the displacement was measured at the load location. The curves are identified as SX-Y, with X referring to the series number (S1, S2 and S3 refer to series #1, series #2 and series #3, respectively) and Y the number of the specimen (from 1 to 7). Note that no results are presented for the specimens S2-6, S2-7 and S3-2 due to a malfunction of the monitoring system.

For the specimens S1(series #1 with 2 rods) presented in Fig. 8a, all the specimens exhibited an elastic response until a bending moment of approximately 10.0 kN·m and a beam displacement of 36 mm. A ductile behaviour was then noted for most of the test. The average peak moment of 11.4 kN·m was reached for a beam displacement of 58 mm in average. After the peak moment, the moment slightly decreased but the displacement largely increased until failure of the steel rod in tension (see Fig. 9) at a displacement of about 124 mm.

Specimen of series #2 (S2) with 4 rods showed similarity with series #1 with 2 rods. As presented in Fig. 8b, specimens S2 exhibited an elastic response until a moment of about 19.8 kN·m and a displacement of 58.1 mm. Then, the specimens S2 exhibited a ductile behaviour. An average peak moment of 21.6 kN·m and a displacement of 133.0 mm were observed. Compared to specimens S1, the specimens S2 exhibited a more important elastic response (larger moment and shear displacement), but in counterpart, the ductile behaviour was less important.

Compared to the specimens of series #1 and #2, the response of the specimens of the series #3 with 8 rods (specimens S3) did not experiences a ductile behaviour. It can be seen on Fig. 8c that the response of specimens S3 is mostly elastic until maximum moment. Near the peak moment, noise and cracking has been heard during the tests. The average moment capacity was 69.1 kN·m and the corresponding displacement was about 98 mm in average. After the peak moment, all samples S3 exhibited a brittle failure. As presented in Fig. 10, failure of the specimens S3 was related to wood splitting rather than steel rupture as observed for specimens S1 and S2 (see Fig. 9).

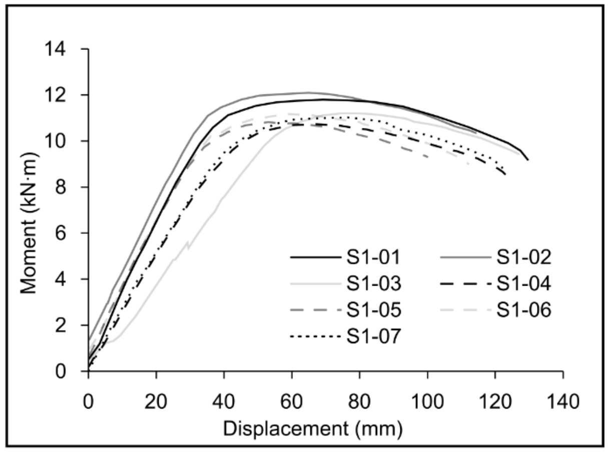

a)

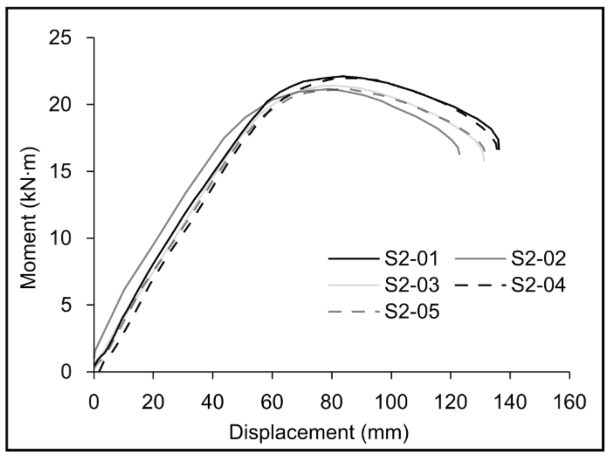

b)

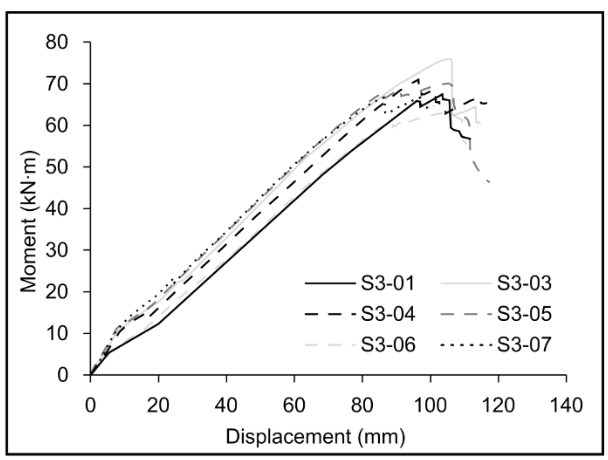

c)

Fig. 8. Moment versus displacement response for a) series #1, b) series #2 and c) series #3

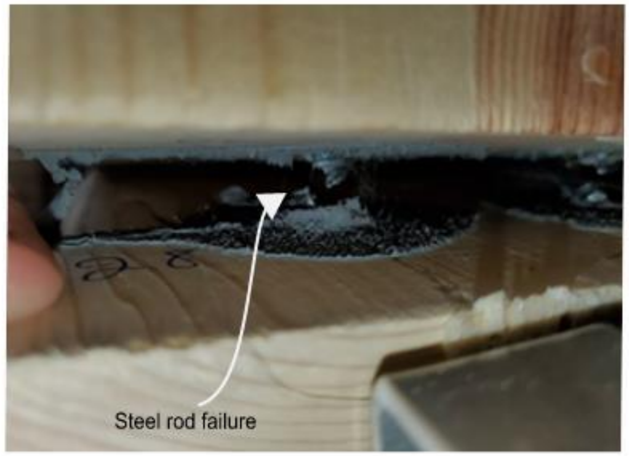

Fig. 9. Failure of the steel rods (series #1 and #2)

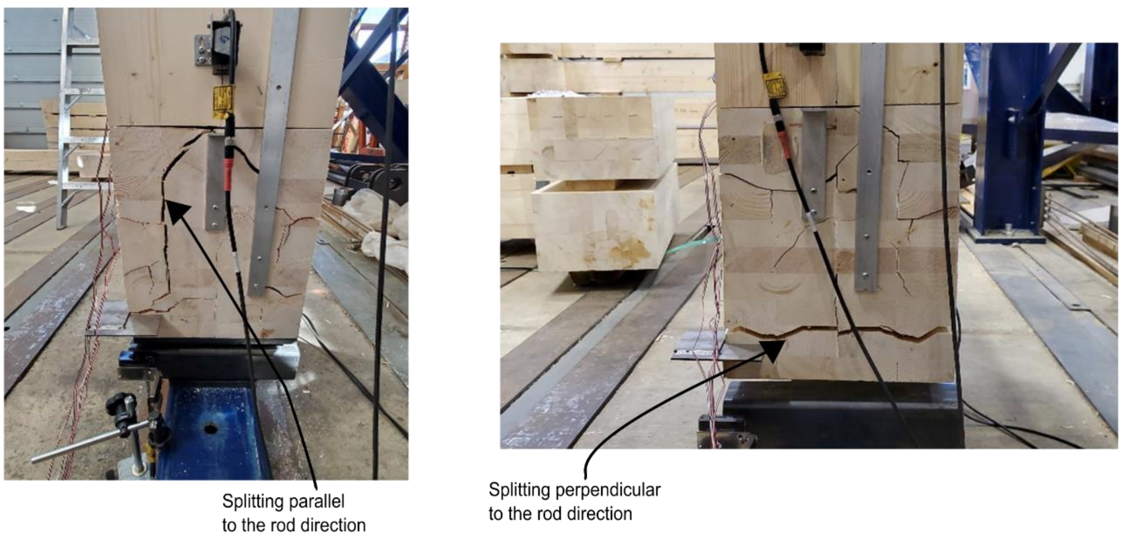

Fig. 10. Brittle failure by wood splitting (series #3)

Bending moment versus joint rotation response

The rotation of the connection was determined using the two lasers positioned on either side of the joint, which are lasers #1 and #2 presented in Fig. 6 and Fig. 11.

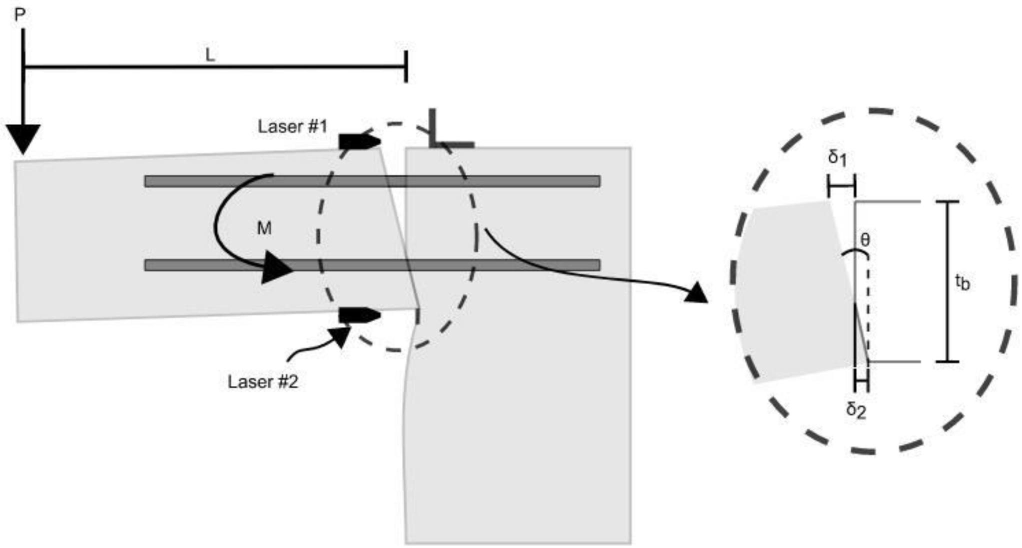

Fig. 11. Rotation measurement

From the dimensions of the member and the measured displacement, the rotation angle of the connection, θ (relative rotation between the beam and the column) can be determined as follows:

$$\theta = arctan\left(\frac{\delta_1 + \delta_2}{t_b}\right) \tag{6}$$

With δ_1 and δ_2 the displacements measured by lasers #1 and #2, respectively. The bending moment versus rotation response is presented in Fig. 12 for each test series. The gray area represents the range of the results for all the tested specimens of the same series. The elastic bending stiffness of the connector was also determined from Fig. 12. To do so, the average slope of the moment versus rotation curve was determined in the elastic behaviour, which was taken between 0 bending moment and 80% of the maximum bending capacity of the connection.

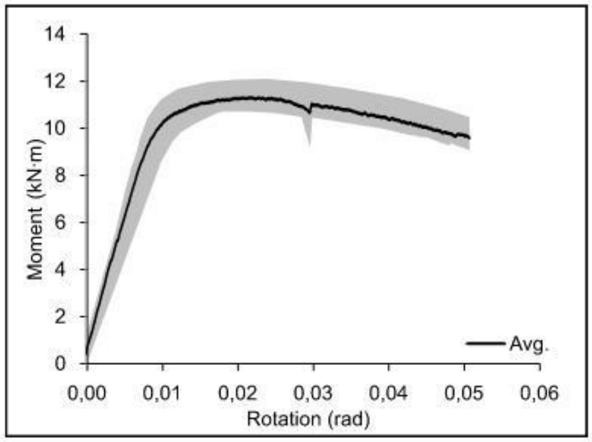

a)

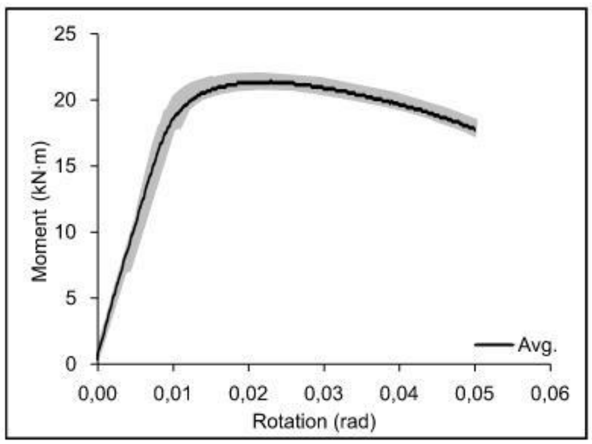

b)

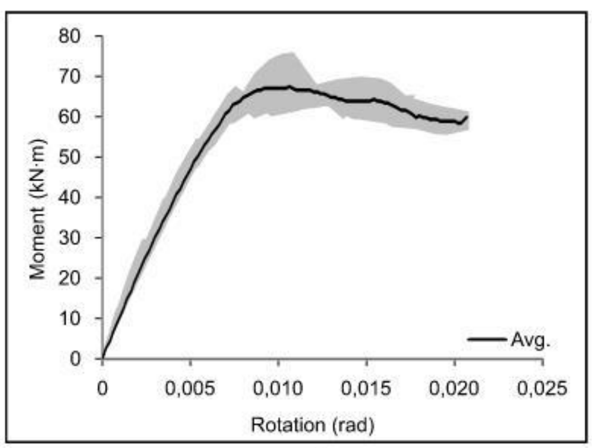

c)

Fig. 12. Bending moment versus rotation response for a) series #1, b) series #2 and c) series #3

The average bending stiffness of the connection determined for each series is presented in Table 6. It can be seen that the connection bending stiffness varies between 1007 and 8303 kN·m/rad, which may be associated to a semi-rigid connection (Beaulieu, Picard et al. 2010). By comparing series #1 and series #2, it can be seen that for the same timber sections and connection geometry, doubling the number of rods doubles the stiffness (1107 kN·m/rad for series #1 with 2 rods compared to 1919 kN·m/rad for series #2 with 4 rods). For series #3, the number of rods il also doubled compared to series #2. However, the rotational stiffness of the connection of the series #3 is about 4 times larger than for series #2 (8303 kN·m/rad compared to 1919 kN·m/rad). That may be explained by the higher and larger timber section at the joint and the resulting longer lever arms of the rods, which increases the connection stiffness. It can therefore be state that, as expected, the bending stiffness of the connection depend on the number of rods and the geometry of the connection.

Table 4. Average rotational stiffness

Series	Number of rods	Rotational stiffness kN·m/rad
#1	2	1107
#2	4	1919
#3	8	8303

Shear displacement response

Fig. 13 presents the shear at the joint versus the relative displacement between the beam and the column at the joint measured with laser #3 (see Fig. 6) for series #1, #2 and #3.

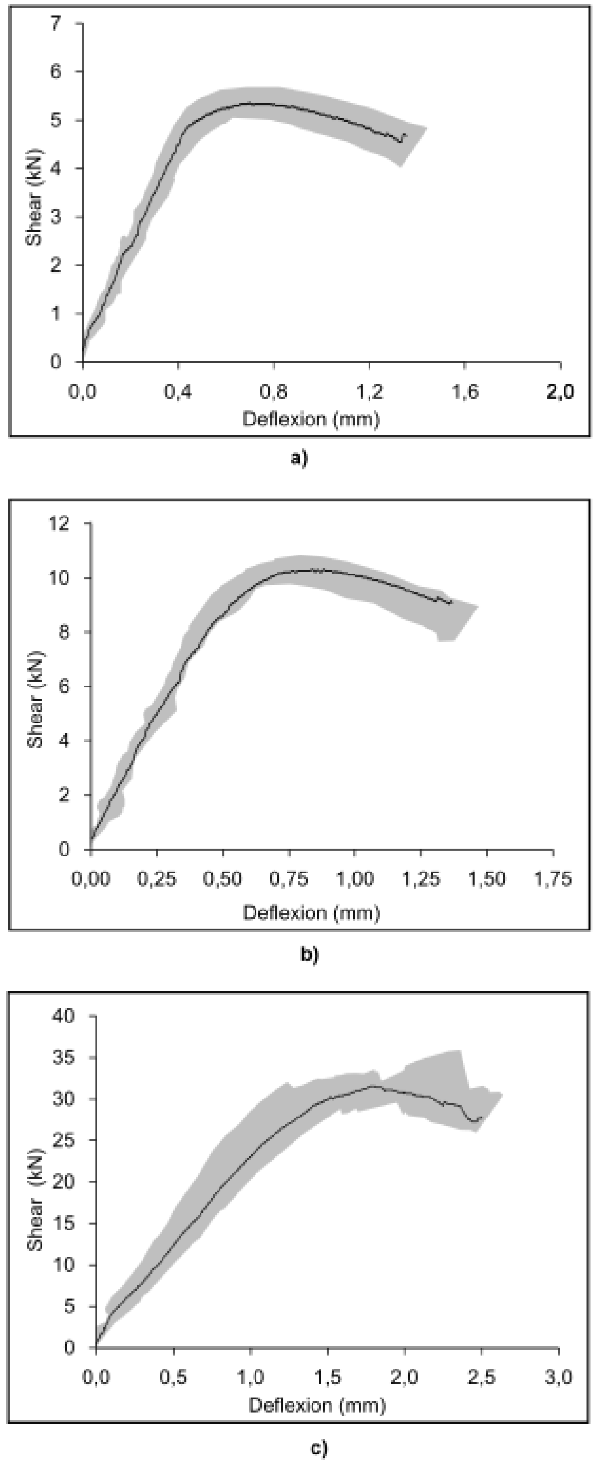

Fig. 13. Shear versus joint displacement response for a) series #1, b) series #2 and c) series #3

It can be seen in Fig. 13 that the relative displacements between the beam and the column at the joint are very limited for all series. All the connections present a significant elastic behaviour up to a displacement of 0.4

mm for series #1, 0.5 mm for series #2 and 1.1 mm for series #3 and a shear of about 90% of the maximum shear for all tests. These displacements are not significant for typical beams compared to codes limitations. For example, according to the Canadian building code (CNRC 2015), a deflection of 21.4 mm is allowed in service for a 7.5 m span beam. A displacement of 1.1 mm therefore represents less than 5% of the allowed value (1.1 mm / 21.4 mm). After reaching about 90% of the connection capacity, the displacement increases up to maximum shear and failure. The displacement increases may be associated to the crushing of the wood causes by the rods bearing and the damage of the anchorage.

As it was the case for the rotational stiffness, a value for the relationship between this deflection and the shear force was determined. The average values are presented in table 6. It can be seen that the stiffness of the specimens with 4 rods (series #2) is about 67% larger than the stiffness of the specimens with 2 rods of the series #1 (17.7/10.6). However, using 8 rods for the series #3 of does not significantly increase the shear stiffness compared to specimens with 4 rods of the series #2 (increase of 16%, 20.6/17.7).

Table 5. Average shear stiffness

Series	Number of rods	Avg. shear stiffness (kN/mm)
#1	2	10.6
#2	4	17.7
#3	8	20.6

Comparison between theoretical and experimental values

Table 7 compares the experimental (exp.) and the predicted (theo.) maximum moment determined with the theoretical model previously presented (see Fig. 3 and Eqs. (1) to (5)). The anchors capacity in Eq. (1) and used to determine the theoretical maximum moments was calculated considering the anchor capacity determined by pull-out tests (see Table 1) and the steel rods failure given by the steel ultimate strength (f_u = 414 MPa for series #1 and #2, and 675 MPa for the test series #3). From Eq. (1), the steel tensile strength of the rods limits the capacity of the anchorages for the series #1 and #2 while, for the series #3, the steel had a much higher ultimate strength so that the capacity of the rods is limited by wood splitting failure.

Table 6. Comparison between experimental and theoretical results (Values in kN·m)

Series	Number of tests	Number of rods	Avg. bending moment to failure			Failure mode	
			Exp.	Theo.	Exp. / Theo.	Exp.	Theo.
1	7	2	11.4	10.0	1.14	Steel yielding	Steel yielding
2	5	4	21.6	19.9	1.07	Steel yielding	Steel yielding
3	6	8	69.1	68.0	1.02	Wood splitting	Wood splitting
Average					1.08		
Coefficient of variation					1.6 %		

It can be seen in Table 7 that experimental results are very consistent with model predictions. The deviation between experimental results and theoretical predictions varies between 1.6% and 12.2% and, on average, the ratio between the theoretical and the experimental capacity is 1.08 (coefficient of variation of 1.6 %), which confirm the model validity. This represents approximately 1 kN·m which is strongly satisfying. For the test series #3, the steel strength of the rods was much larger than the steel used for the rods in specimens of the series #1 and #2. Therefore, the model predicts wood splitting failure as experimentally observed. It can be however noted that, considering the same steel used for series #1 and #2 (f_u = 473.4 MPa), the model predicts a ductile failure associated to the steel yielding and a maximal bending moment of 57.3 kN·m for the specimens of the series #3.

Stress distribution in the different components of the connection

The strain gauges installed on the rods directly at the joint between the beam and the column were used to determine the load carried by each component of the connection (rods and wood). From the measured strain, ε_s, the average steel stress, σ_s was determined for rods from the following equations (Palermo and Vecchio 2002).

$$\sigma_s = \begin{cases} E_s \cdot \varepsilon_s \leq f_y, & |\varepsilon_s| \leq \varepsilon_{sh} \\ f_u + (f_y - f_u)\left(\dfrac{\varepsilon_u - \varepsilon_s}{\varepsilon_u - \varepsilon_{sh}}\right)^4, & otherwise \end{cases} \tag{7}$$

Considering the net area of each rod, the force carried by the rods in compression and in tension was calculated using Eqs. (3) and (4). By considering equilibrium, the difference between tension and compression was attributed to the wood. The determined contribution of each component for series #2 and #3 is presented according to the applied moment in Fig. 14. For comparison purposes, the theoretical value determined with the model is also presented (identified “Theo.” in Fig. 14). Note that the results of the series #1 is not presented since there were no strain gauges installed on the rod in compression to determine its force component. Also, only one of the rods was monitored for each rod layer of the series #3, so that the total force in tension and in compression may be taken as twice the load carried by one rod in Fig. 14b.

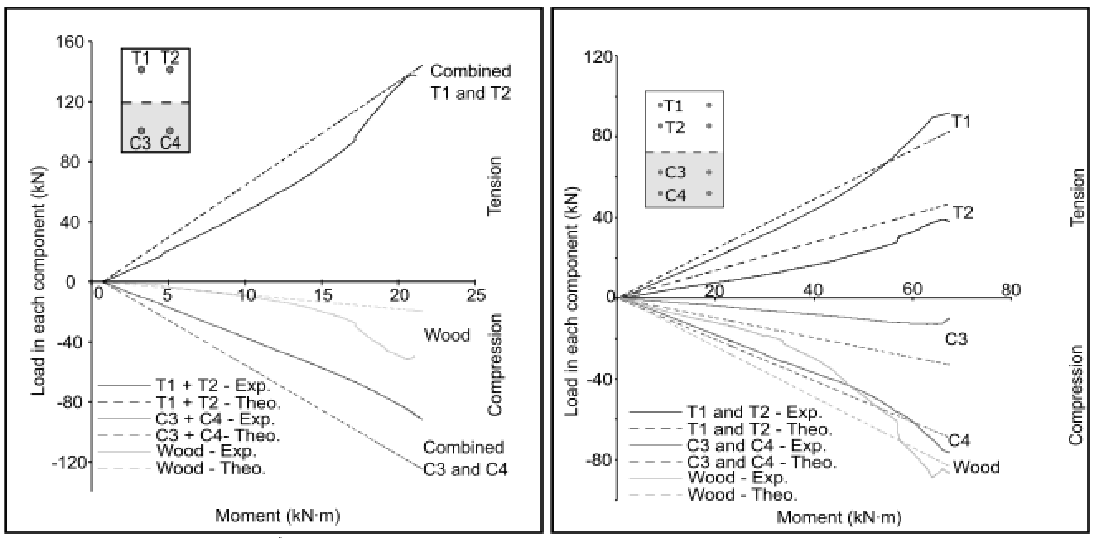

a) b)

Fig. 14. Comparison between experimental (Exp.) and theoretical (Theo.) load in each component for a) series #2 and b) series #3

It can be seen in Fig. 14 that the difference between the experimental and theoretical values is relatively small, confirming the relevance of the calculation model as well as the reliability of the experimental method.

It may be determined that the steel used for series #1 and #2 with f_u = 473.4 leads to an ultimate force of 132.8 kN (2 rods carrying 66.4 kN each). That confirms that the failure occurred after the rupture of steel rods in tension. For the series #3, the tensile strength of the steel, f_u, was 675 MPa leading to an ultimate force of 98.4 kN for one rod. However, as presented in Table 1, the tensile capacity of the anchorage was limited by the wood splitting capacity of 81.8 kN. As presented in Fig. 14b, 91.7 kN was carried by the rods T1 at the connection failure, which is below the steel tensile strength of the rod (98.4 kN) and match the wood capacity determine with pull-out tests (81.8 kN). It can also be predicted that, with the same rod capacity of 66.4 kN for the steel used for series #1 and #2, series #3 would have exhibit a ductile failure caused by steel rupture instead of wood splitting, reaching an average maximal bending moment of 55.2 kN·m. These results showed that the connection can exhibit a ductile failure mode when wood splitting capacity must be larger than steel capacity of rods.

Stress distribution along the anchor

On the specimens of series #1, 5 strain gauges were installed along the steel rod working in tension to study the steel strain distribution and the anchorage efficiency. Fig. 15 presents the stress along a rod in tension for a typical specimen of the test series #1 (refer to Fig. 7 and Fig. 16 for gauges numbering the rod exact location). The stress was obtained from the measured strain in accordance with Eq. (7). For comparison, the theoretical axial stress determined at the joint using Eqs. (2) to (5) is also presented in Fig. 15 and identified as ‘’Theo. stress at the joint’’.

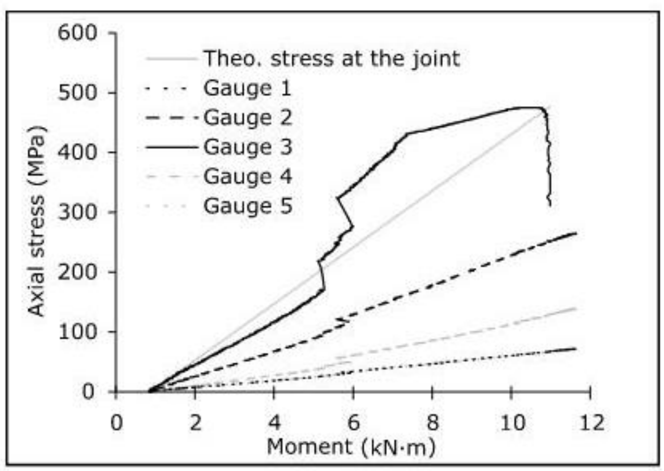

Fig. 15. Axial stress in the rods versus moment on a typical specimen of the series #1 determined from the strain gauge measurement along the rod in tension

As expected, it can be observed that the maximum axial stress occurs at the joint between the beam and the column (gauge #3) and decreases away from the joint. For the rod at the joint, a moment of 6.2 kN·m caused steel yielded (σ_s > f_y = 410 MPa), while the rod failed in tension for a moment of 11.1 kN·m. The other locations away from the joint exhibited an elastic behaviour, with a measure strain below f_y = 410 MPa.

Fig. 16 presents the rod axial stress and the bond stress determined from the axial strain along the rod at failure of the member. The axial stress was determined from Eq. 7 while the bond stress, τ, correspond to the slope of the axial stress along the bar, Δ_σ/Δ_L, given as follows.

$$\tau = \frac{\Delta_\sigma}{\Delta_L}\left(\frac{d_b}{4}\right) \tag{8}$$

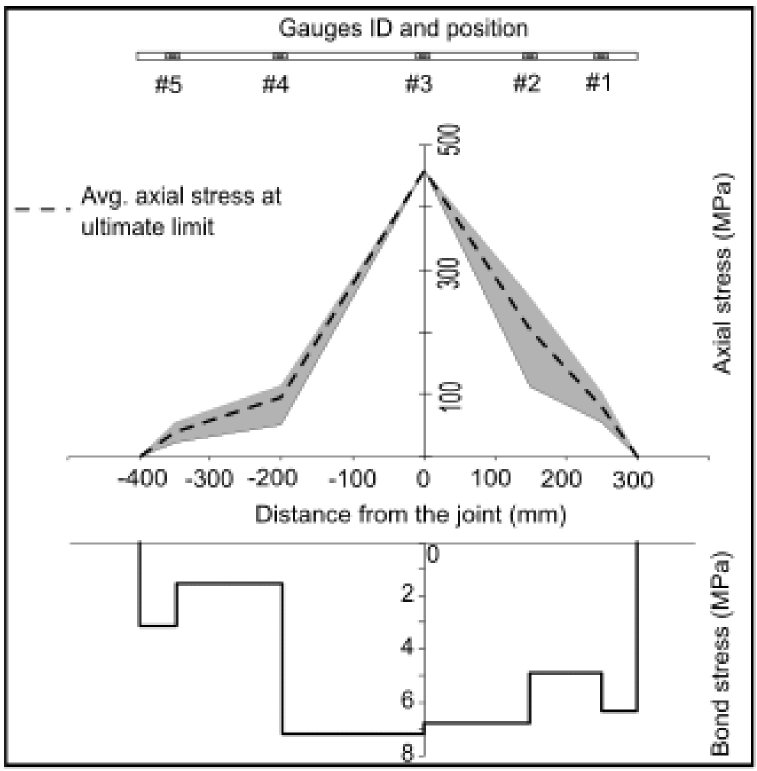

Fig. 16. Stress distribution along the anchorage, typical specimen of series #1

It can be seen that axial stress decreases rapidly near the joint on both sides of the rod. This rapid decay corresponds to a large bond stress of 7.2 MPa on the left side of the joint and 6.8 MPa on the right side of the joint. Thereafter, the decay continues to the right of the joint (column), up to the end of the rod. To the left of the joint (beam), this decrease in axial stress is less important. This is because less adhesion is required due to the higher length of the rod (400 mm in the beam and 300 mm in the column). This explains a lower decrease in the axial stress. Thus, it can be observed for the rod shown in Fig. 16 that the bond stress is relatively uniform along the rod for a length of 300 mm. On the opposite, an increase in the length of the rod to 400 mm leads to a less uniform bond stress.

Conclusion

In this paper, three series of true scale glued-in rods beam-column moment-resisting connections were tested and their behaviour investigated.

The main conclusions are the following:

1. For the tested glued-in rods beam-column connections, the behaviour and the capacity of the connections are a function of the number of rods, their configuration, the steel properties of the rods and the wood splitting capacity. Increasing the number of rods or their lever arm increase the connection stiffness and capacity. The tested connections exhibited a semi-rigid behaviour in bending.
2. Results showed that the connection exhibited a ductile failure mode and residual capacity after the peak moment when its failure was caused by yielding and rupture of the steel rods, i.e. when the splitting capacity of the wood was larger than the tensile capacity of the steel rods in tension. Otherwise, a brittle failure of the connection with a limited residual moment capacity after the peak load was observed when wood splitting occurred first.
3. For the tested specimens, the vertical deflection at the junction between the beam and the column was negligible compared to the typical beam deflection and the maximal deflection generally allowed by building codes.
4. In the connection, the moment is carried by the rods in tension, the rods in compression and the wood in compression. Test results showed that the contribution of wood in compression is not negligible, may reaching about 30% of the force in compression. It is therefore recommended to consider the wood contribution in compression for the design of glued-in rods moment-resisting connection.
5. Strain gauges were installed along the embedded rod, on each side of the joint, to study axial and bond stresses. Prior to the bar failure at the joint, results indicated that the bond stress was mostly uniform along the short-embedded part of the rod (embedment of 300 mm). For the larger embedded part of the rod (embedment of 400 mm), the stress distribution in the anchorage was non-uniform, with a larger bond stress near the joint and at the rod extremity. The stress distribution in the

anchorage is non-uniform. The analytical models indicating stress concentration were confirmed by the results obtained from the strain gauges on series #1 samples.

6. Comparison between the theoretical model predictions and the experimental results indicated good agreement, in term of connection capacity and load carried by each component of the connection.
7. For design, it is recommended that the engineers limit the steel capacity or provide rod embedment and rod cover large enough so that the failure of the connection occurs by rupture of the steel rod in tension instead of wood splitting. Thus, a ductile failure of the connection is expected.

Results and conclusions presented in this paper will help safely using and design this type of connection. In addition, results can be used as a comparison basis in the development of design rules for glued-in rods connections in the near future.

Data availability statement

Some or all data, models, or code that support the findings of this study are available from the corresponding author upon reasonable request:

- Gross results;
- Photos;
- Technical information on the components of the testing set-up.

Acknowledgements

The authors are grateful to Natural Sciences and Engineering Research Council of Canada for the financial support through its IRC and CRD programs (IRCPJ 461745-18 and RDCPJ 524504-18) as well as the industrial partners of the NSERC industrial chair on eco-responsible wood construction (CIRCERB).

References

ASTM (2016a). Standard Test Methods for Tenstion Testing of Metallic Materials. **ASTM E8-E8M**.

ASTM (2017a). Standard Practice for Establishing Clear Wood Strength Values. **ASTM D2555**.

ASTM (2019). Standard Test Methods for Cyclic (Reversed) Load Test for Shear Resistance of Vertical Elements of the Lateral Force Resisting Systems for Buildings. **ASTM E2126**.

ASTM (2021). Standard Specification for Carbon Steel Bolts, Studs, and Threaded Rod 60 000 PSI Tensile Strength. **ASTM A307**.

Beaulieu, D., Picard, A., Tremblay, R., Grondin, G. and Massicotte, B. (2010). Calcul des charpentes d'acier - Volume 2, Canadian Institue of Steel Construction.

Bédard-Blanchet, G. (2014). Système d'attache métallique pour poutres lamelléescollées. Saint-Jean-Port-Joli, Art Massif - Structure de bois.

Brassard, D. (2018). Le bois remplace lentement l'acier. Radio-Canada.

Cecobois (2018). "Le bois atteint de nouveaux sommets." Construire en bois **10**(2).

CNRC (2015). Code national du bâtiment - Canada. Ottawa, Conseil national de recherches du Canada. **1 and 2**.

CSA (2019). Règle de calcul des charpentes en bois. **O86-19**.

DIN (2012). Entwurf, Berechnung und Bemessung von Holzbauwerken – Allgemeine Bemessungsregeln und Bemessungsregeln für den Hochbau. **1052**.

Fragiacomo, M. and Batchelar, M. (2012). "Timber Frame Moment Joints with Glued-In Steel Rods. I: Design." Journal of Structural Engineering **138**(6): 789-801.

Gauthier-Turcotte, E., Menard, S., Fiset, M. and Chang, W.-S. (2021). Pull-out Strength of Glued-in Steel Rod Perpendicular to the Grain in Spruce-Pine Glulam TimberR. World Conference on Timber Engineering 2020. Santiago, Chile.

Hassanieh, A., Valipour, H. R., Bradford, M. A. and Jockwer, R. (2018). "Glued-in-rod timber joints: analytical model and finite element simulation." Materials and Structures **51**(3).

Inoue, J., Uetsuki, K., Sato, N., Kei, T. and Inoue, M. (2018). Pull-Out and Moment Resisting Test of Glued-In Rod Joint Using Toughness Metal Connector. 2018 World Conference on Timber Engineering. Seoul, Republic of Korea.

Kajikawa, H., Hiraga, S. and Ogawa, H. (2018). Study of Pull-Out Strength of Glued-in Rod Joints. WCTE. Seoul, Republic of Korea.

Klapwijk, D. (1978). "RESTORATION AND PRESERVATION OF DECAYED TIMBER STRUCTURES AND CONSTRUCTIONS WITH EPOXIES." Studies in Conservation **23**(sup1): 75-76.

Lartigau, J. (2013). Caractérisation du comportement des assemblages par goujons collés dans les structures bois Thèse, Université Bordeaux 1.

Loctite (2015). LOCTITE® CR 421 PURBOND - Fiche Technique.

Oh, J. (2016). Timber Moment Connections Using Glued-In Steel Rods Mémoire, University of British-Columbia.

Ouellet, M.-C. (2013). Rapport d'analyse des tests de traction sur les tiges d'acier collées dans le bois. Québec, Université Laval.

Palermo, D. and Vecchio, F. J. (2002). Behaviour and Analysis of Reinforced Concrete Walls Subjected to Reversed Cyclic Loading, University of Toronto

Simonin (2008). Avis Technique - Goujons collés RESIX, CSTB**:** 15.

Stepinac, M. (2013) "Comparison of design rules for glued-in rods and design rule proposal for implementation in European standards." Timber specific publishing.

Stepinac, M., Bidakov, A., Jockwer, R. and Vlatka, R. (2018). Review and Evaluation of Design Approaches for Glued-In Rods in East and West Europe. 2018 World Conference on Timber Engineering, Seoul, Republic of Korea.

Tlustochowicz, G., Serrano, E. and Steiger, R. (2010). "State-of-the-art review on timber connections with glued-in steel rods." Materials and Structures **44**(5): 997-1020.

Vasek, M. (2008). Semi rigid timber frame and space structure connections by glued-in rods. 10th WCTE, Miyazaki, Japan.

Verdet, M. (2017). Étude du comportement à long terme de systèmes d'assemblages par goujons collés en conditions climatiques variables Université Laval et Université de Bordeaux.

Verslype, J. (2016). Caractérisation d'un dispositif d'assemblage en bois de type tiges collées en pied de poteau. Québec, Université Laval**:** 212.

Widmann, R., Steiger, R. and Gehri, E. (2007). "Pull-out strength of axially loaded steel rods bonded in glulam perpendicular to the grain." Materials and Structures **40**(8): 827-838.